nature synthesis

Article

https://doi.org/10.1038/s44160-022-00167-5

Highly compressible and environmentally adaptive conductors with high-tortuosity interconnected cellular architecture

In the format provided by the authors and unedited

Supplementary Information

Highly compressible and environmentally adaptive conductors with high-tortuosity interconnected cellular architecture

Yangyu Wang[1], Haili Qin[1], Zheng Li[1], Jing Dai[1], Huai-Ping Cong[1]* & Shu-Hong Yu[2]*

[1]*School of Chemistry and Chemical Engineering, Hefei University of Technology, 230009, P. R. China*

[2]*Department of Chemistry, Institute of Biomimetic Materials & Chemistry, Division of Nanomaterials and Chemistry, Hefei National Research Center for Physical Sciences at the Microscale, University of Science and Technology of China, 230026, P. R. China*

Correspondence should be addressed to the author: H. P. C. (hpcong@hfut.edu.cn) or S. H. Y. (shyu@ustc.edu.cn).

Supplementary Methods

Materials. CNTs (10-20 nm in diameter and 10-30 μm in length) and SiO_2NWs (40-60 nm in diameter and 80-100 μm in length) were purchased from Nanjing XFNANO Materials Tech Co., Ltd and used as received. PEDOT:PSS (1.1% in H_2O, high-conductivity grade) was purchased from Sigma-Aldrich Co. and used without further purification. Other chemicals were purchased from Sinoparm Co., Ltd.

Synthesis of CuNWs. The CuNWs with 60-100 nm in diameter and 70 μm in length were synthesized by a modified hydrothermal method[1]. Typically, 0.084 g of $CuCl_2 \cdot 2H_2O$ and 0.099 g of glucose were dissolved in 40 mL of water. Under stirring, 0.54 g of 1-hexadecylamine (HDA) was added and stirred for 10 h at room temperature until the solution turned into a light blue emulsion. Then, the above emulsion was transferred into a Teflon-lined stainless-steel autoclave and reacted at 120 ^{o}C for 10 h. Finally, the resulting CuNW products were rinsed with hot water (60℃) to remove excess HDA and glucose.

Synthesis of GONSs. The GONSs were synthesized by a modified Hummers' method[2]. Firstly, 5 g of flake graphite and 3.75 g of $NaNO_3$ were added into a 1000 mL beaker with gentle stirring. With slowly adding into 160 mL of concentrated H_2SO_4 and stirring for 0.5 h, the solution turned into black color. Then, 20 g of $KMnO_4$ was added into the above suspension at a slow rate. With stirring for 20 h, the mixture was gradually thickened with the diminishing in effervescence. After aging for 5 days, 500 mL of water was slowly added into the paste, leading to violent effervescence. Finally, the suspension was treated with 30 mL of H_2O_2 and the suspension turned into bright yellow color. After centrifugally washed, the GONSs were collected and dialyzed for 7 days to remove the impurities.

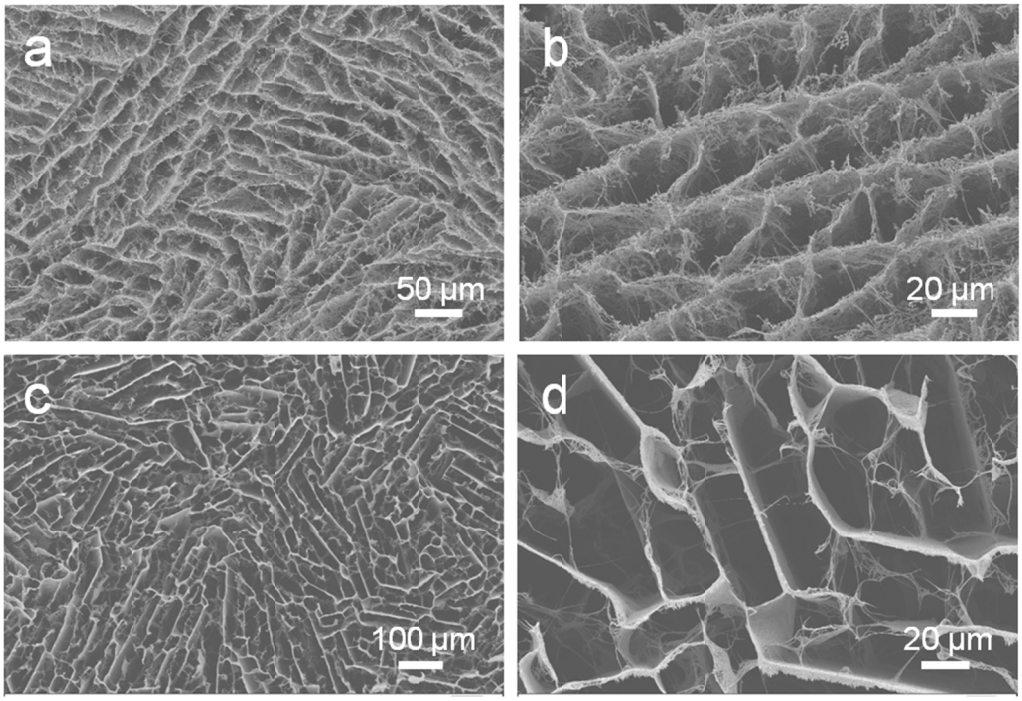

Supplementary Figure 1. SEM images with different magnifications of directional freezing of (**a, b**) the AgNW-containing polymerisable solution and (**c, d**) AgNW dispersion at -120 °C. The monolith presented a refined cellular microstructure composed of AgNW film-assembled compartmental units with homogenous pore size of ~20 μm. For comparison, the bare AgNW aerogel fabricated by directional freezing exhibited a cellular shape with the pore length of ~25 μm and width of ~50 μm in random distribution.

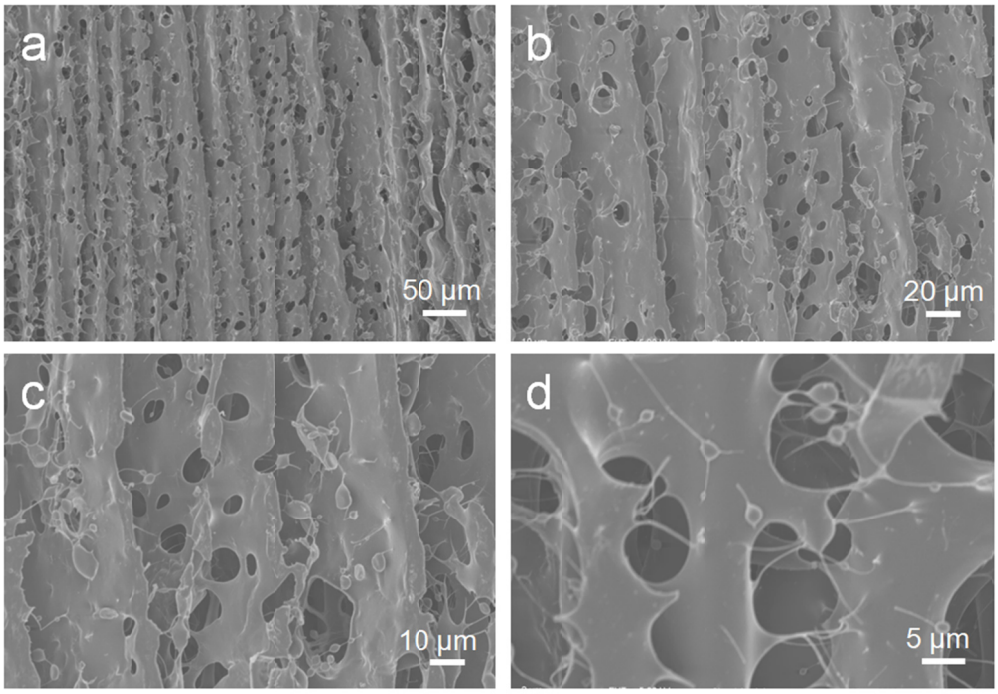

Supplementary Figure 2. SEM images with different magnifications for time-dependent evolution of the CCAP hydrogel during the cryopolymerization process for 2 h.

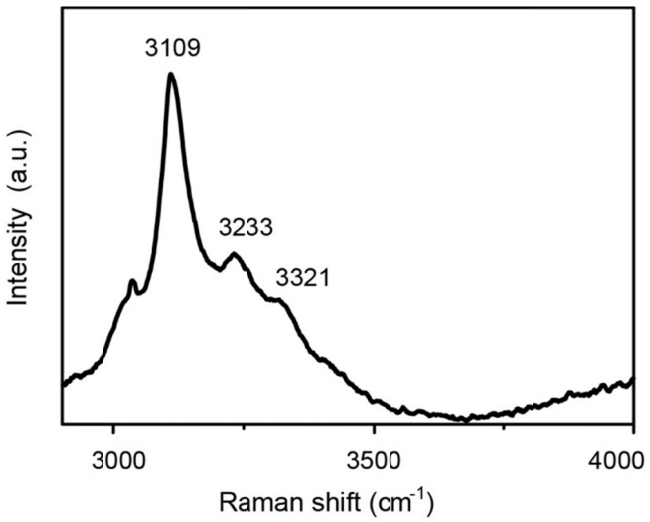

Supplementary Figure 3. Cryo-raman spectra of the precursor solution for the fabrication of CCAP hydrogel recorded at -120 °C. For the directional freezing-assembly at -120 °C, the liquid water molecules in the monolith were frozen into ices, as indicated by the symmetric and antisymmetric O-H stretching vibrations at 3321 cm^{-1} and 3109 cm^{-1} and an overtone band at 3233 cm^{-1} for the hexagonal ice (ice I*h*) in Raman spectrum.

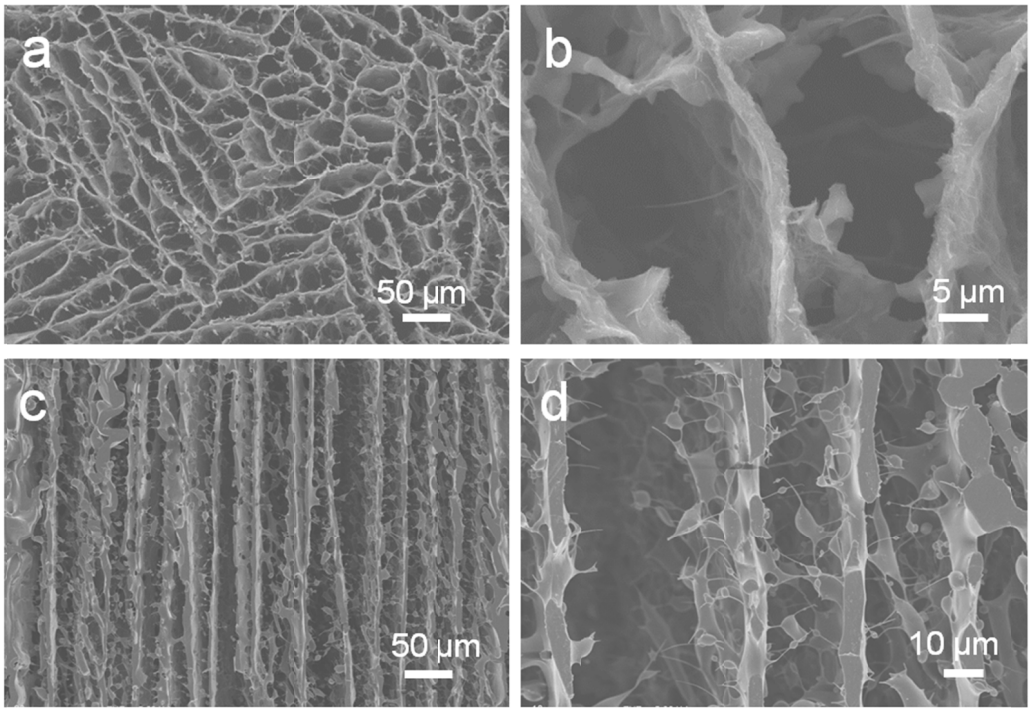

Supplementary Figure 4. SEM images with different magnifications for time-dependent evolution of the CCAP hydrogel during the cryopolymerization process for 12 h. (**a, b**) Top-view images, and (**c, d**) side-view images.

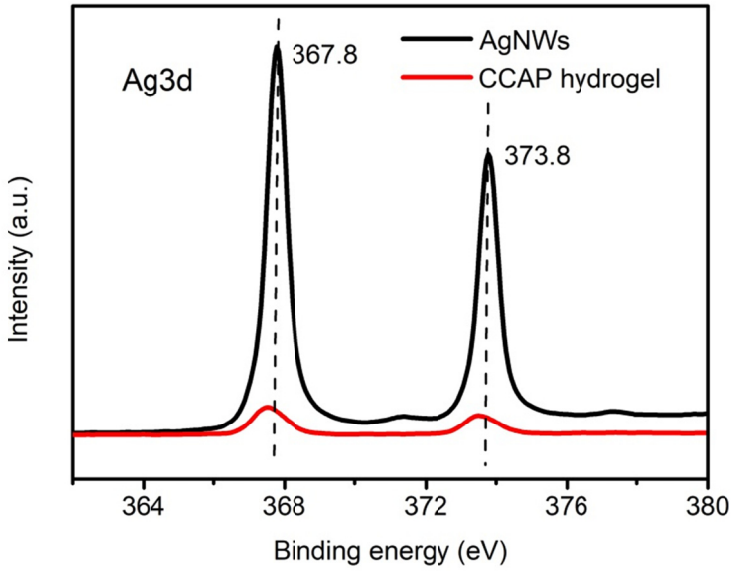

Supplementary Figure 5. XPS spectra of Ag3d peaks of AgNWs and CCAP hydrogel. In the Ag3d XPS spectra, compared with the bare AgNWs, the red-shifts of the two characteristic peaks of Ag3d3/2 at 367.8 eV and Ag3d5/2 at 373.8 eV suggested the formation of the Ag-N bonds between AgNWs and PAM chains.

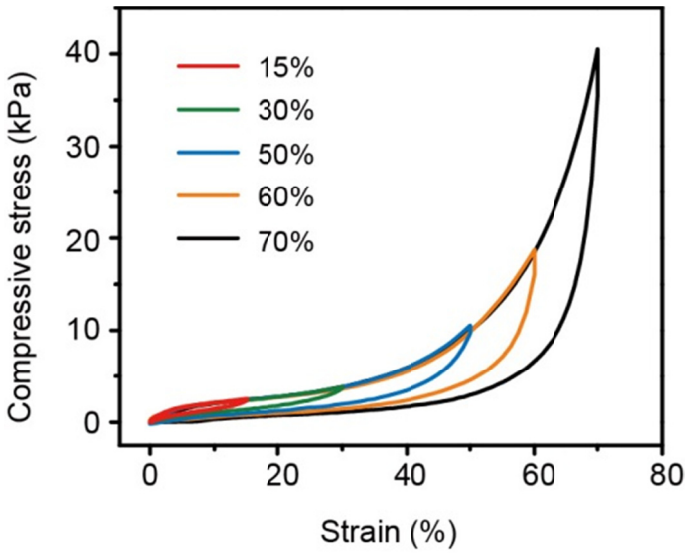

Supplementary Figure 6. Loading-unloading stress-strain curves of the CCAP hydrogel at different compressive strains in air.

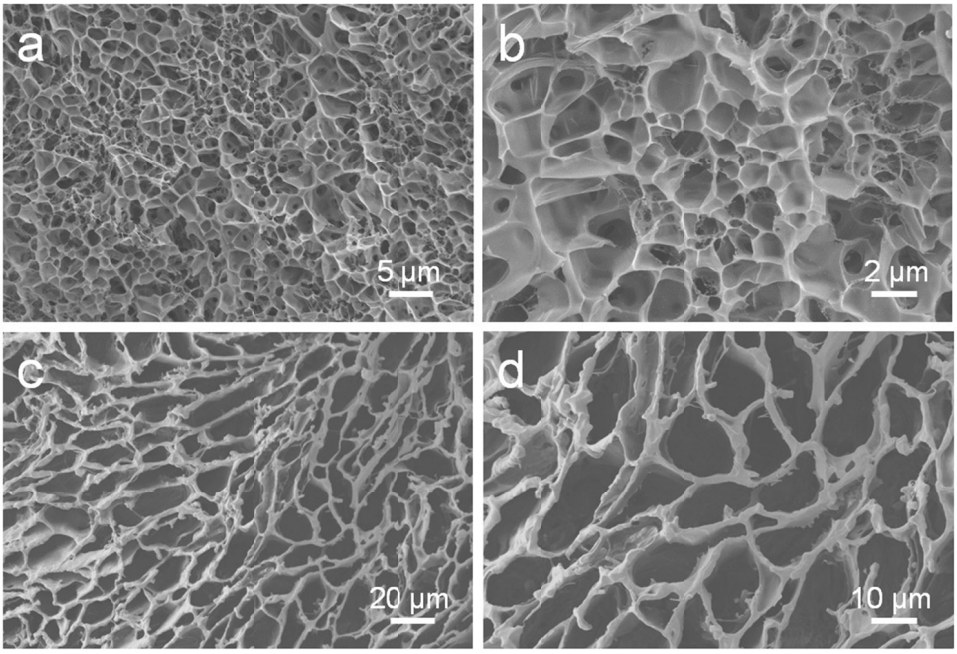

Supplementary Figure 7. SEM images with different magnifications of (**a, b**) AgNW/PAM and (**c, d**) DF-PAM hydrogels.

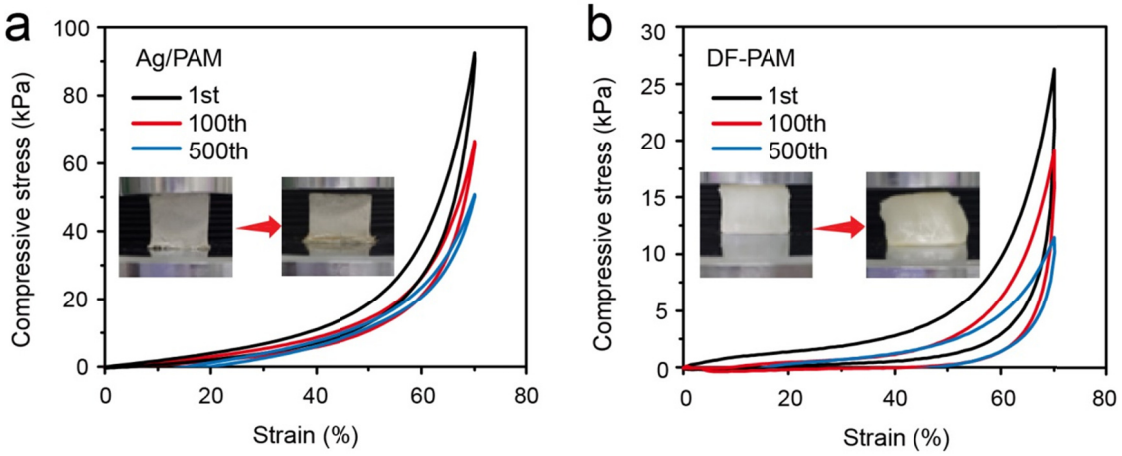

Supplementary Figure 8. Compressive stress-strain curves of (**a**) Ag/PAM hydrogel and (**b**) DF-PAM hydrogel under cyclic compression. The inserted photographs show the corresponding hydrogels before and after 500 compression cycles.

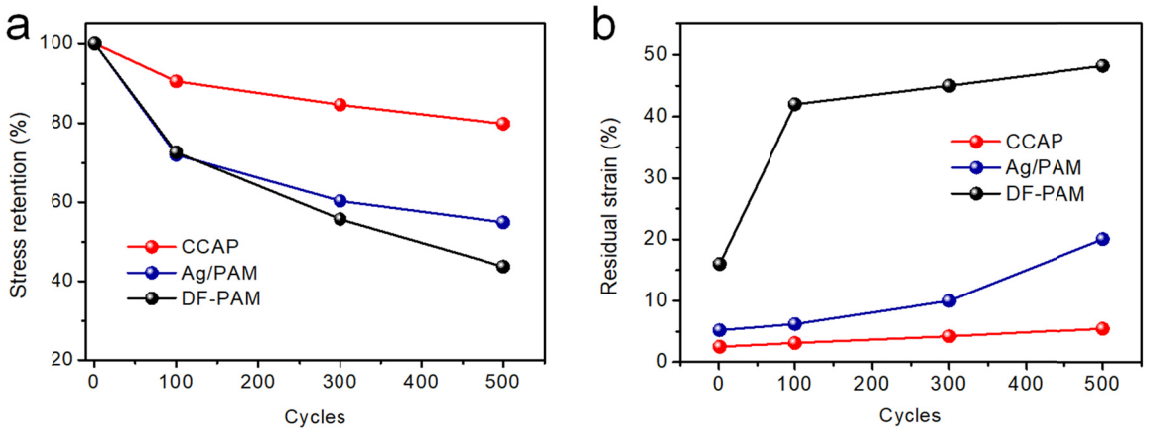

Supplementary Figure 9. Changes of (**a**) maximum stress and (**b**) residual strain of the CCAP, Ag/PAM and DF-PAM hydrogels during 500 cycles at 70% strain in air.

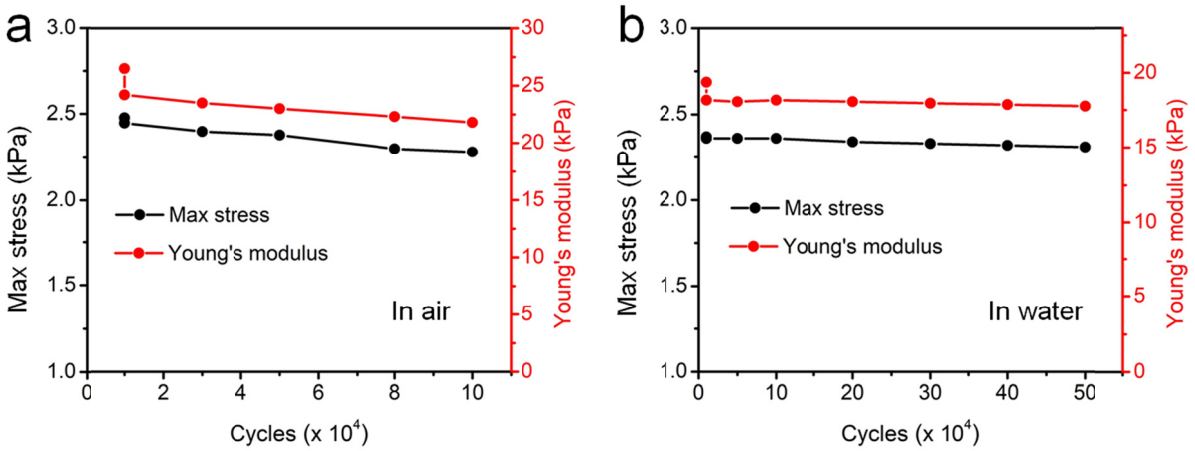

Supplementary Figure 10. Changes of maximum stress and Young's modulus of the CCAP hydrogel during 1×10^5 cycles at 15% strain in air (**a**) and during 5×10^5 cycles at 15% strain in water (**b**).

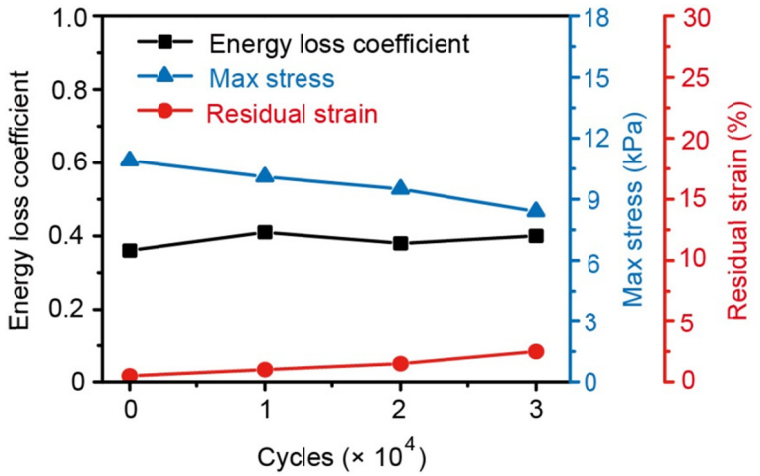

Supplementary Figure 11. Changes of energy loss coefficient, maximum stress and residual strain of the CCAP hydrogel during 3×10^4 cycles at 50% strain in air.

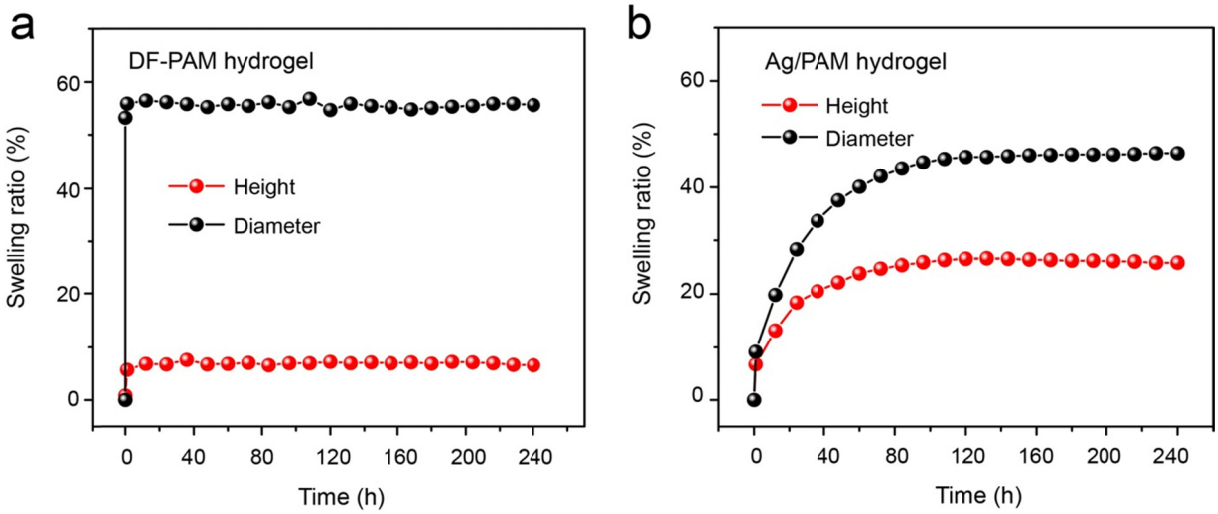

Supplementary Figure 12. Swelling ratio curves of the height and diameter against time for (**a**) DF-PAM hydrogel and (**b**) AgNW/PAM hydrogel with the height of 1.3 cm and diameter of 1.1 cm. Relying on free channels, the DF-PAM hydrogel was saturated with water in 10 s, showing 7.5% and 56.5% increase in height and diameter, respectively (Fig. S12a). In contrast, the Ag/PAM hydrogel presented isotropic, omnidirectionally expanded swelling behavior with 27% and 45% increase in height and diameter (Fig. S12b).

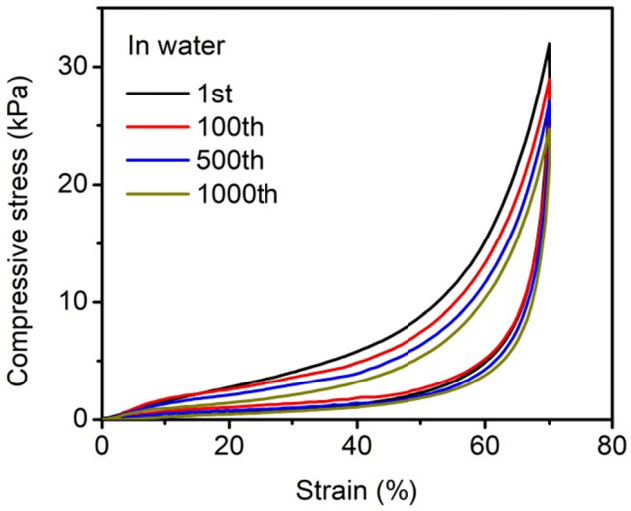

Supplementary Figure 13. Compressive stress-strain curves of the CCAP hydrogel at 70% strain for 1000 cycles in water.

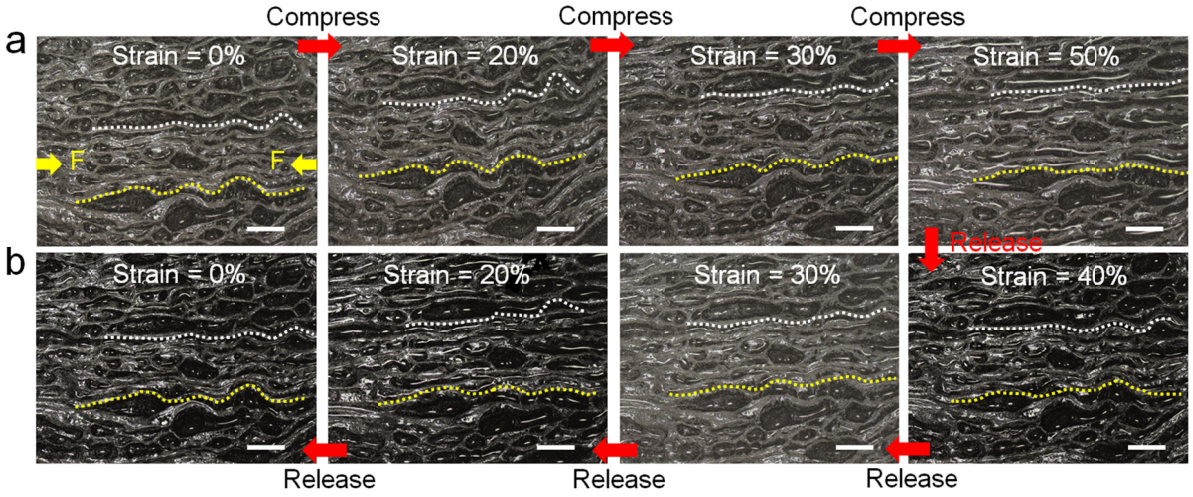

Supplementary Figure 14. *In situ* laser scanning images of side-view structural changes of the CCAP hydrogel (**a**) upon continuous compression to maximum strain of 50% and (**b**) releasing the compressive strains. Scale bar: 200 μm.

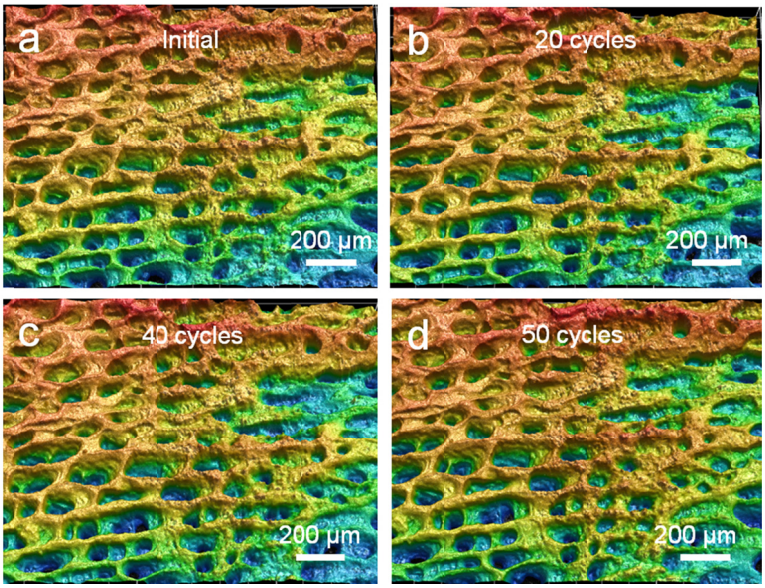

Supplementary Figure 15. Three-dimensional laser scanning profiles of side-view structure of the CCAP hydrogel after cyclic compression at 50% strain. (**a**) 0 cycle, (**b**) 20 cycles, (**c**) 40 cycles and (**d**) 50 cycles.

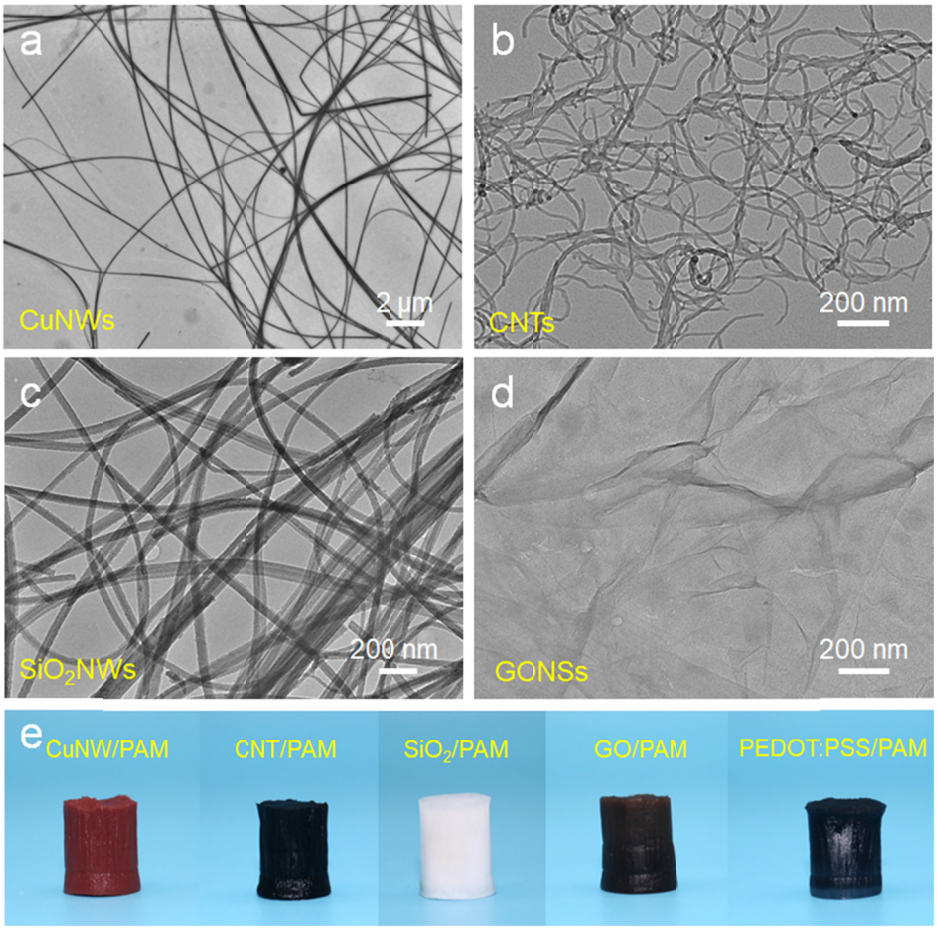

Supplementary Figure 16. TEM images of different assembly units. (**a**) CuNWs, (**b**) CNTs, (**c**) SiO_2NWs and (**d**) GONSs. (**e**) Optical images of the synthesized five hydrogels of CuNW/PAM, CNT/PAM, SiO_2/PAM, GO/PAM and PEDOT:PSS/PAM.

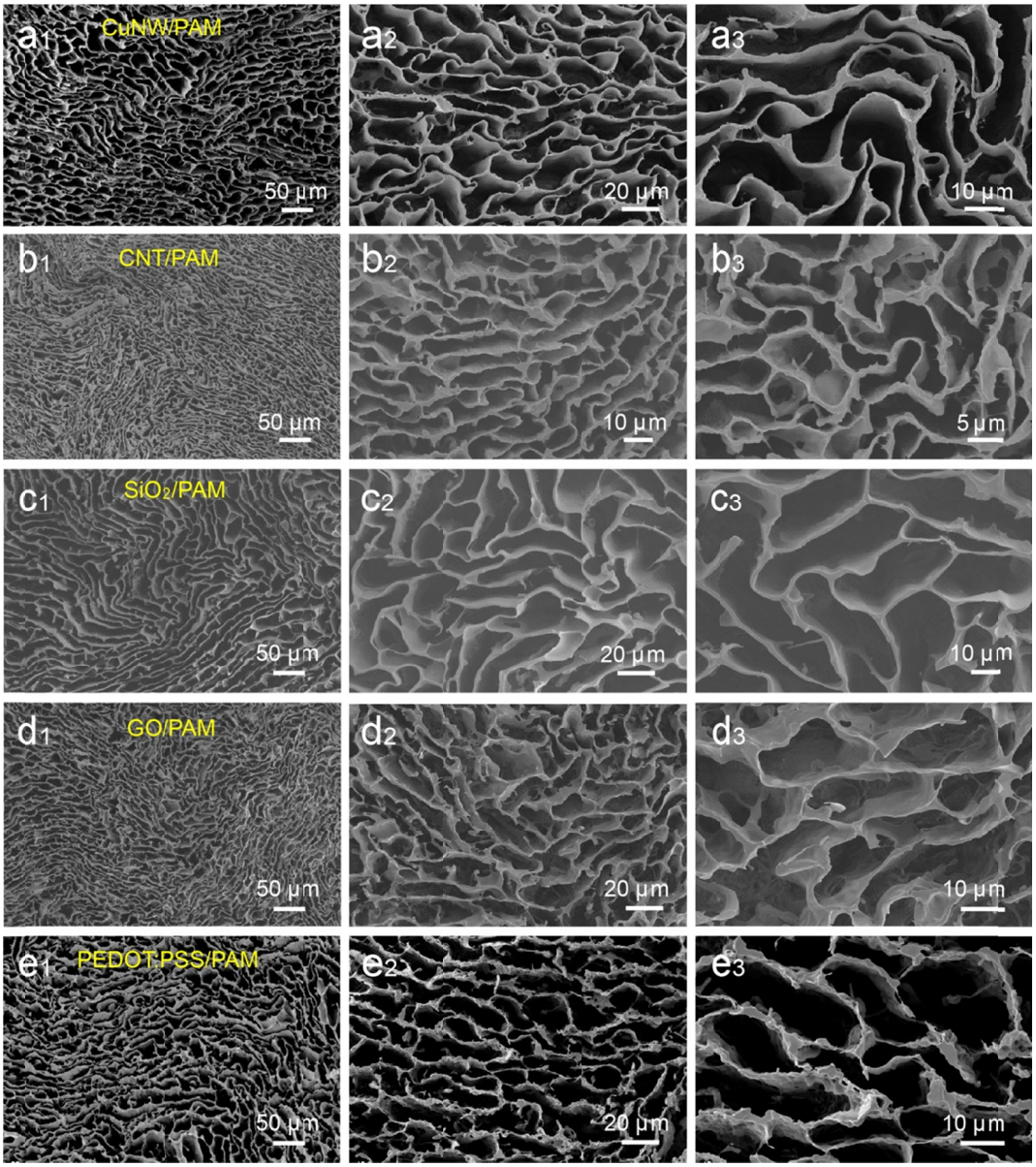

Supplementary Figure 17. Top-view SEM images with different magnifications of five hydrogels. (**a_1-a_3**) CuNW/PAM, (**b_1-b_3**) CNT/PAM, (**c_1-c_3**) SiO_2/PAM, (**d_1-d_3**) GO/PAM and (**e_1-e_3**) PEDOT:PSS/PAM hydrogel. These hydrogels exhibited high-tortuosity endoplasmic reticulum-like structure as that the CCAP hydrogel assembled with AgNWs behaved.

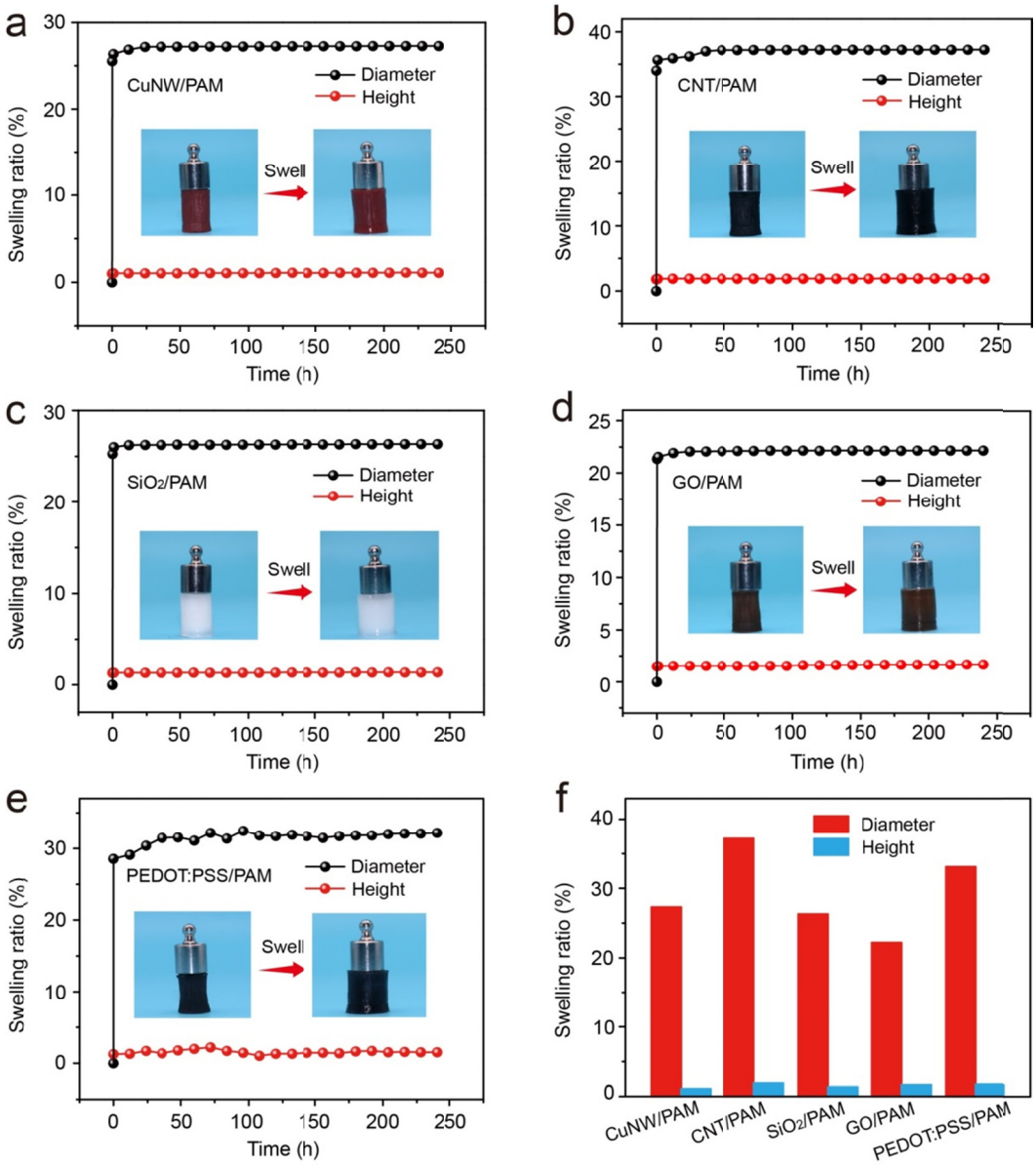

Supplementary Figure 18. Time-dependent swelling ratios of five hydrogels in height and diameter. (**a**) CuNW/PAM, (**b**) CNT/PAM, (**c**) SiO_2/PAM, (**d**) GO/PAM and (**e**) PEDOT:PSS/PAM. The inserted photographs show the corresponding hydrogel with the height of ~ 1.3 cm and diameter of ~ 1.1 cm enduring a weight of 5 g after 10 day of swelling in water. (**f**) Summary of swelling ratios of five hydrogels in height and diameter after swollen in water for 10 day. These hydrogels achieved swelling equilibrium within 10 s with 22%-37% of diameter expansion but negligible variation in height, demonstrating their rapid and highly anisotropic swelling behaviors.

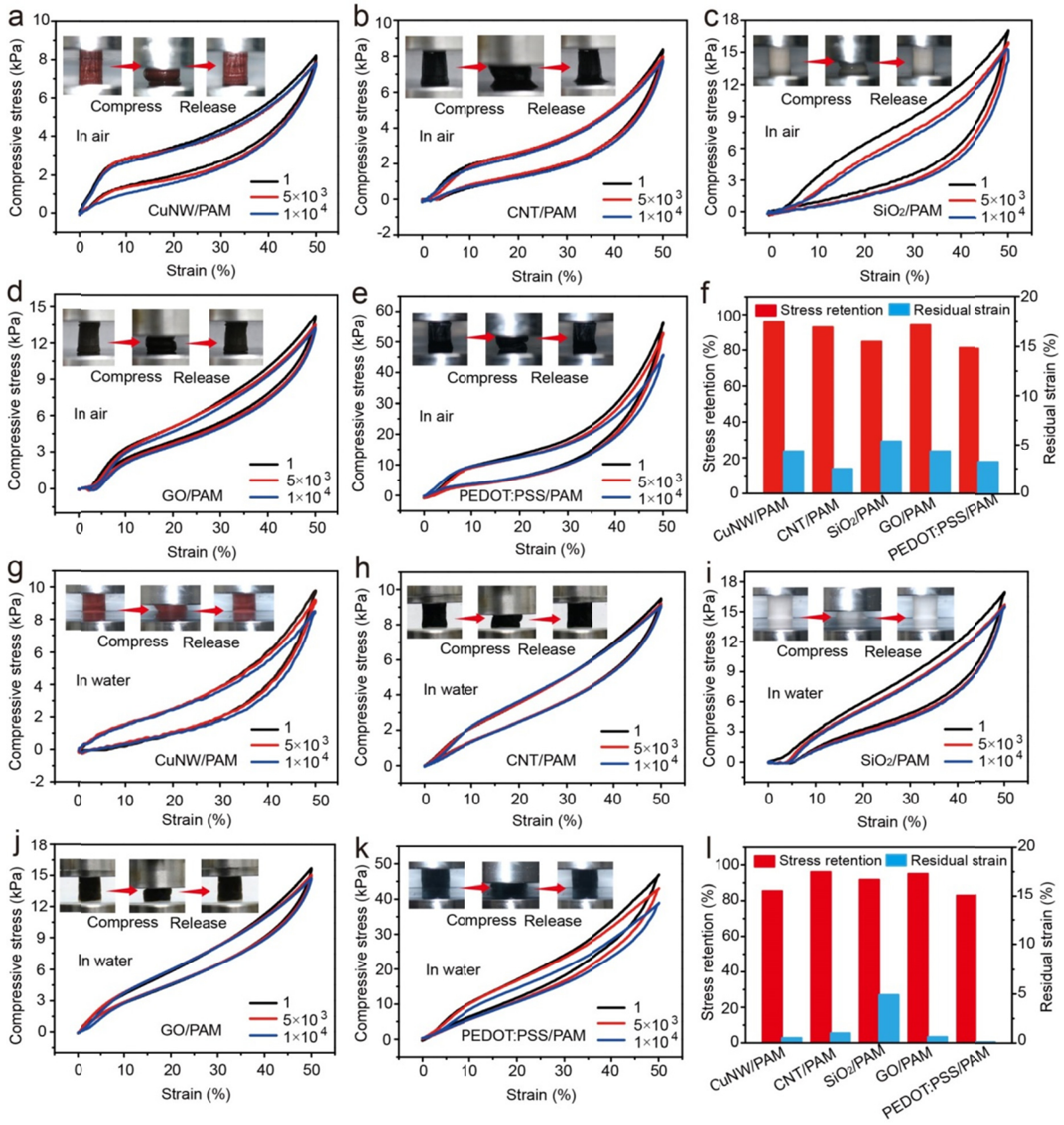

Supplementary Figure 19. Compressive stress-strain curves of different hydrogels at 50% strain for 10^4 cycles in air (**a-e**) and in water (**g-k**). (**a, g**) CuNW/PAM, (**b, h**) CNT/PAM, (**c, i**) SiO_2/PAM, (**d, j**) GO/PAM and (**e, k**) PEDOT:PSS/PAM. The inserted photographs show the corresponding hydrogel recovering to its initial state once releasing the compressive loading. Maximum stress retention and residual strain of varied hydrogels after 10^4 cycles at 50% strain in air (**f**) and in water (**l**). Applied with a compressive strain of 50% for 10^4 cycles in air, the hydrogels showed highly consistent compression profiles with 81.3%-95.7% of maximum stress maintained and small residual strains (2.5%-5.3%). Upon similar cyclic compressive tests in water, the nearly-overlapped compressive curves were recorded with 4.9%-17% decrease in maximum stress and ~ 1% of irreversible strain over 10^4 cycles.

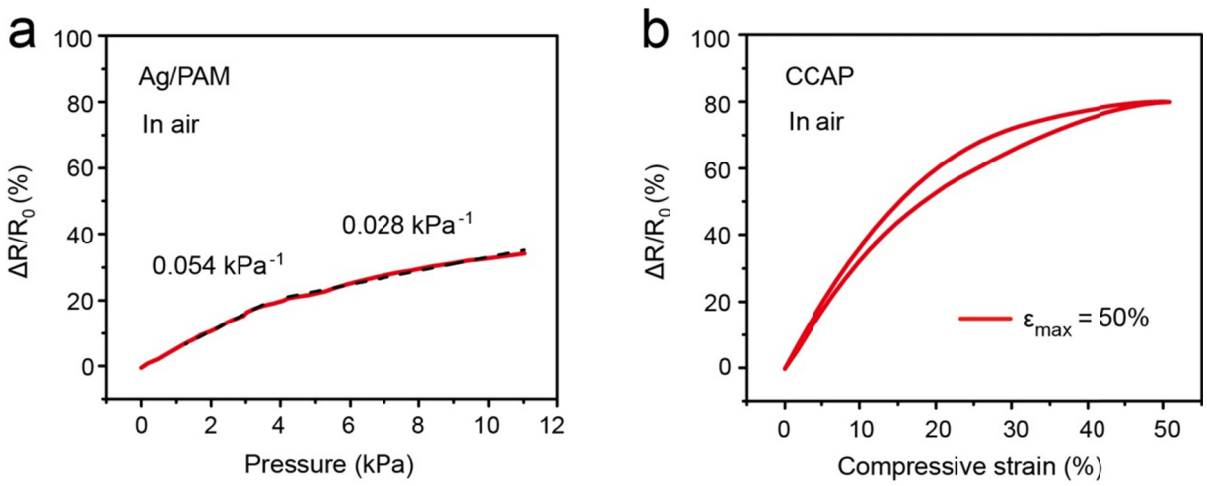

Supplementary Figure 20. (**a**) $\Delta R/R_0$ versus pressure of the Ag/PAM hydrogel in air. (**b**) $\Delta R/R_0$ versus strain the CCAP hydrogel during a compressive cycle in air.

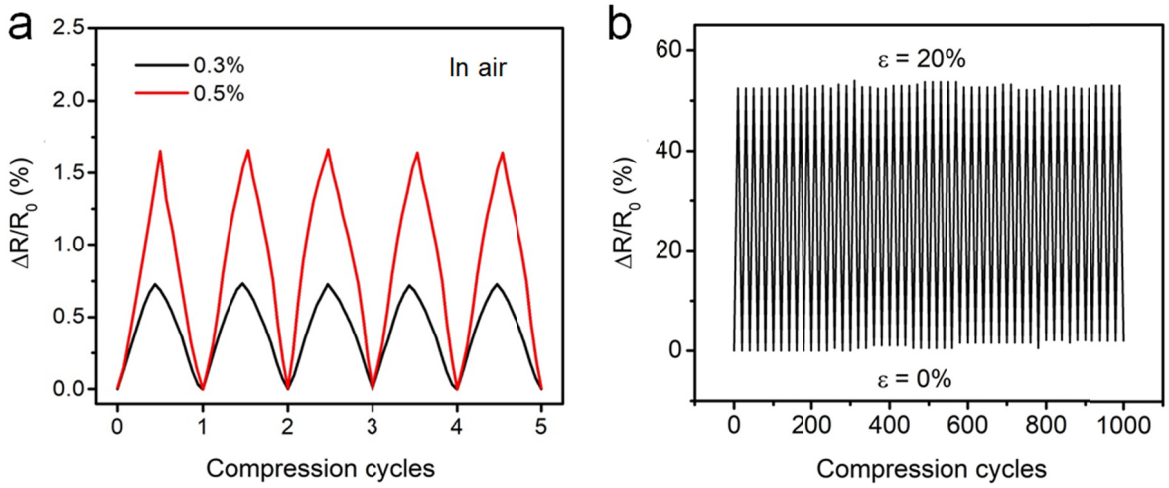

Supplementary Figure 21. (**a**) $\Delta R/R_0$ of the CCAP hydrogel during 5 compression cycles at 0.3% and 0.5% strains in air. (**b**) $\Delta R/R_0$ during 1000 compression cycles at 20% strain in air.

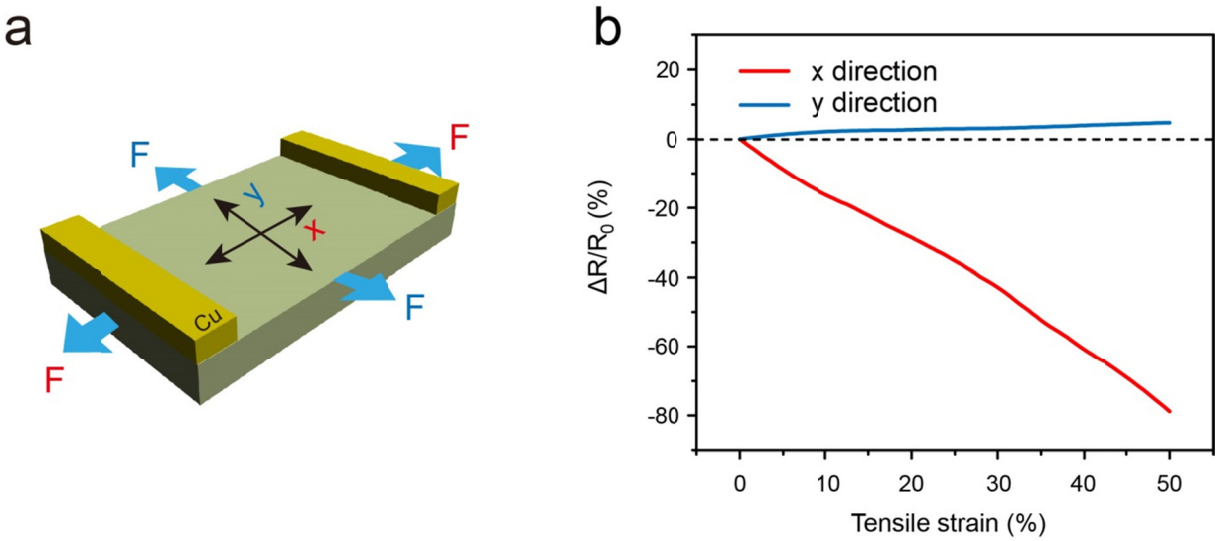

Supplementary Figure 22. (**a**) Schematic illustration show the tensile strains parallel and vertical to the electric current denoted as *x* and *y* direction, respectively. (**b**) $\Delta R/R_0$ of the CCAP hydrogel to the tensile strain in *x* and *y* directions.

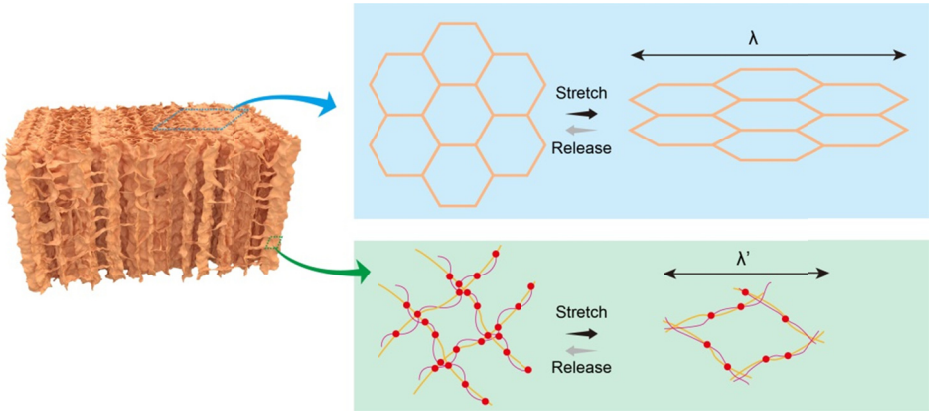

Supplementary Figure 23. Schematic illustrations for the energy-dissipating mechanism of the CCAP hydrogel maintaining the stable conductive network under the stretch.

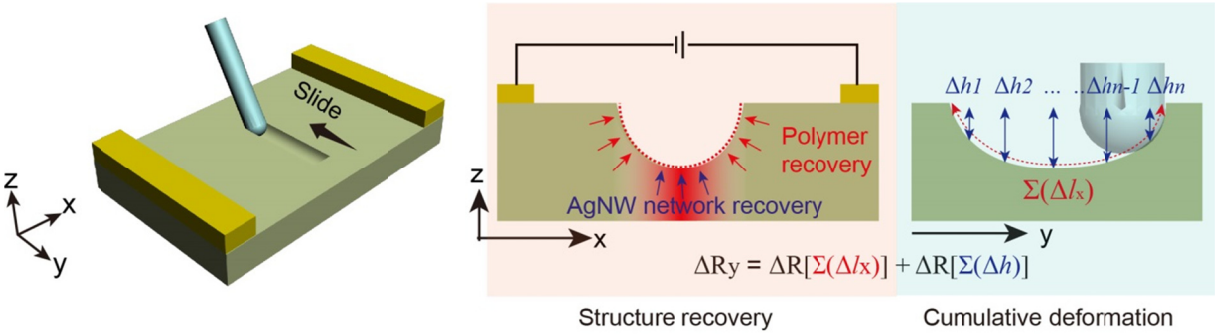

Supplementary Figure 24. Schematic illustrations of the cumulative deformation and structure recovery under the sliding motion in *y* direction.

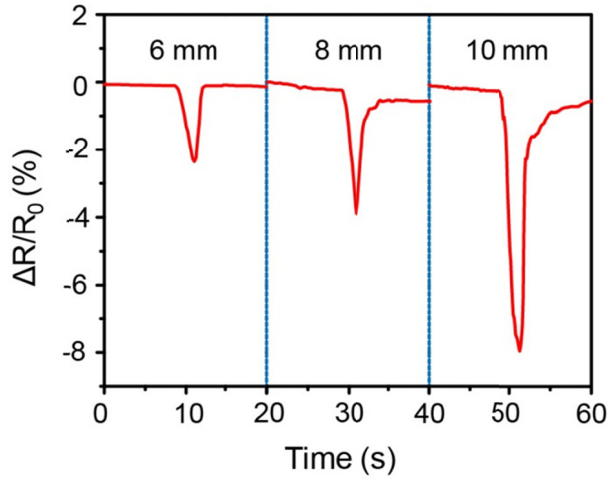

Supplementary Figure 25. $\Delta R/R_0$ of the CCAP hydrogel when pressing its surface to a fixed depth of 1 mm by the glass rods with the diameters of 6 mm, 8 mm and 10 mm, respectively.

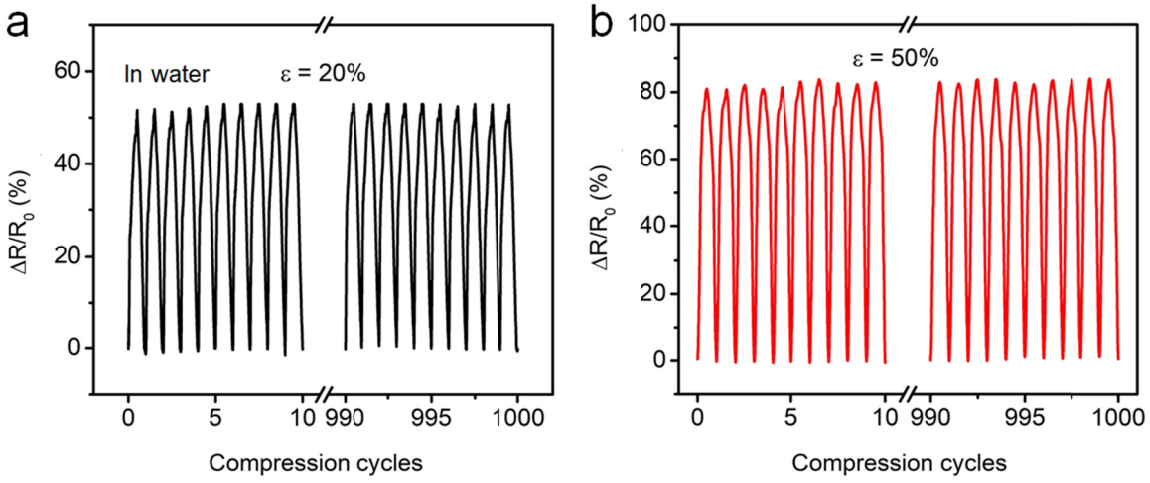

Supplementary Figure 26. $\Delta R/R_0$ during 1000 compression cycles at (**a**) 20% and (**b**) 50% strains in water.

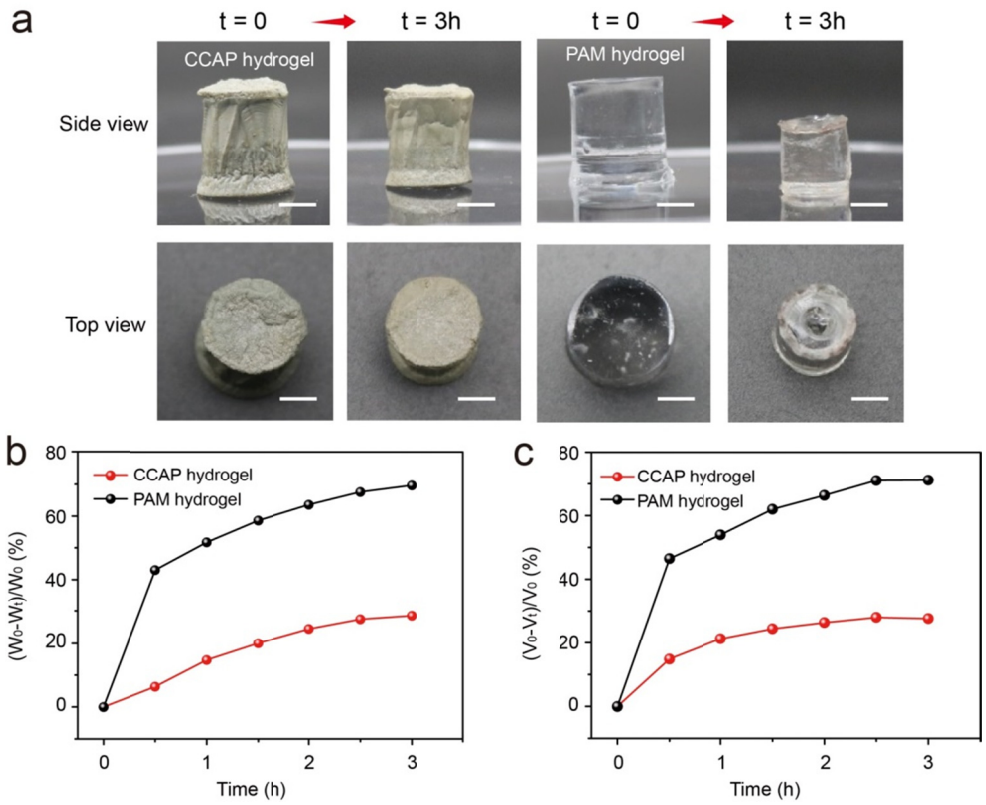

Supplementary Figure 27. (**a**) Side-view and top-view optical images of the CCAP (water content: 87.3%) and PAM hydrogels (water content: 89.2%) before and after soaking in ethanol for 2 h. Scale bars: 5 mm. Normalized weight changes (**b**) and normalized volume changes (**c**) of the CCAP and PAM hydrogels with the time soaking in ethanol.

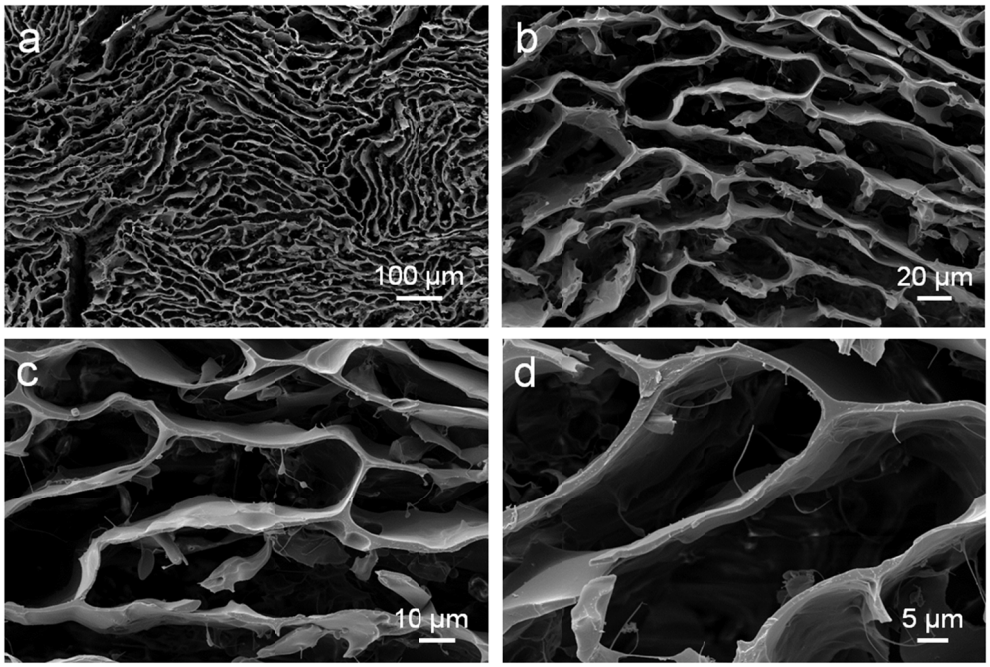

Supplementary Figure 28. Top-view SEM images with different magnifications of the CCAP-based organohydrogel.

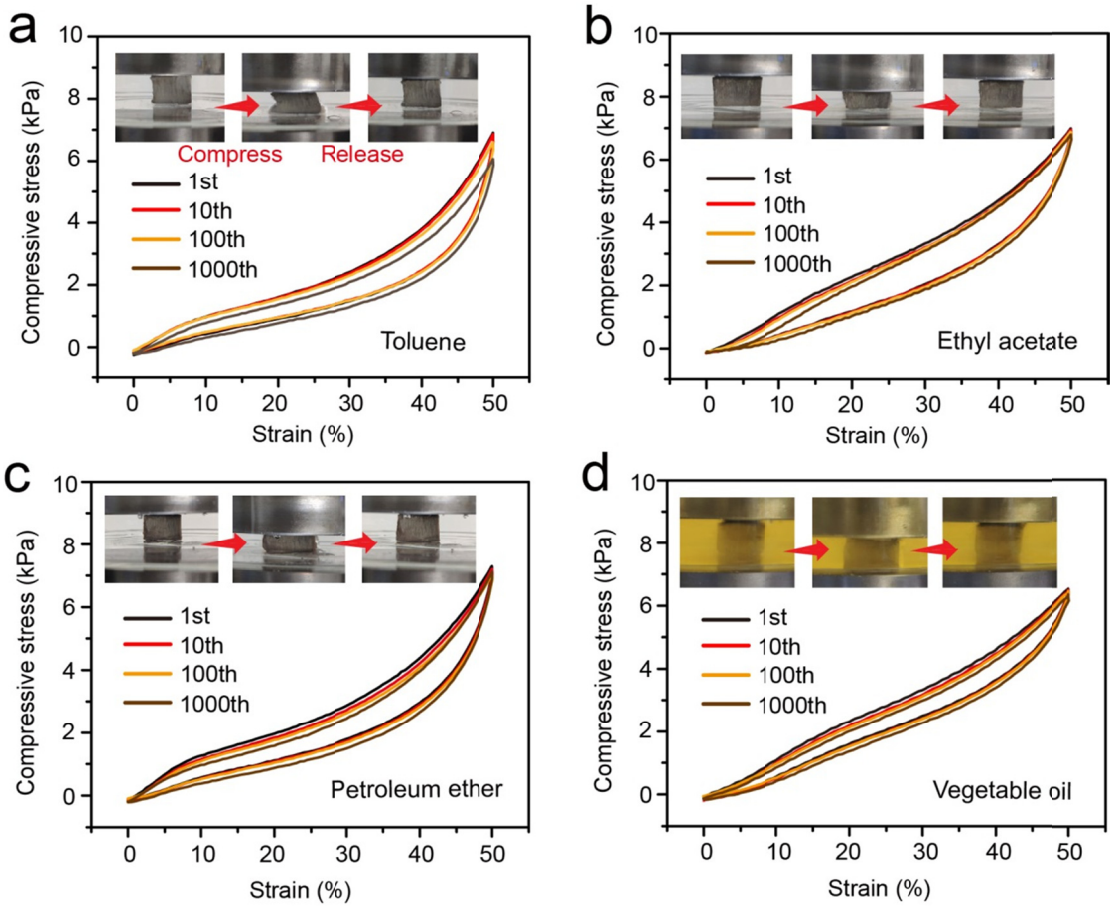

Supplementary Figure 29. Compressive stress-strain curves of the hydrogel in toluene (**a**), ethyl acetate (**b**), petroleum ether (**c**) and vegetable oil (**d**) under cyclic compression. The inserted photographs show the hydrogels recovering the initial shapes upon releasing the compression.

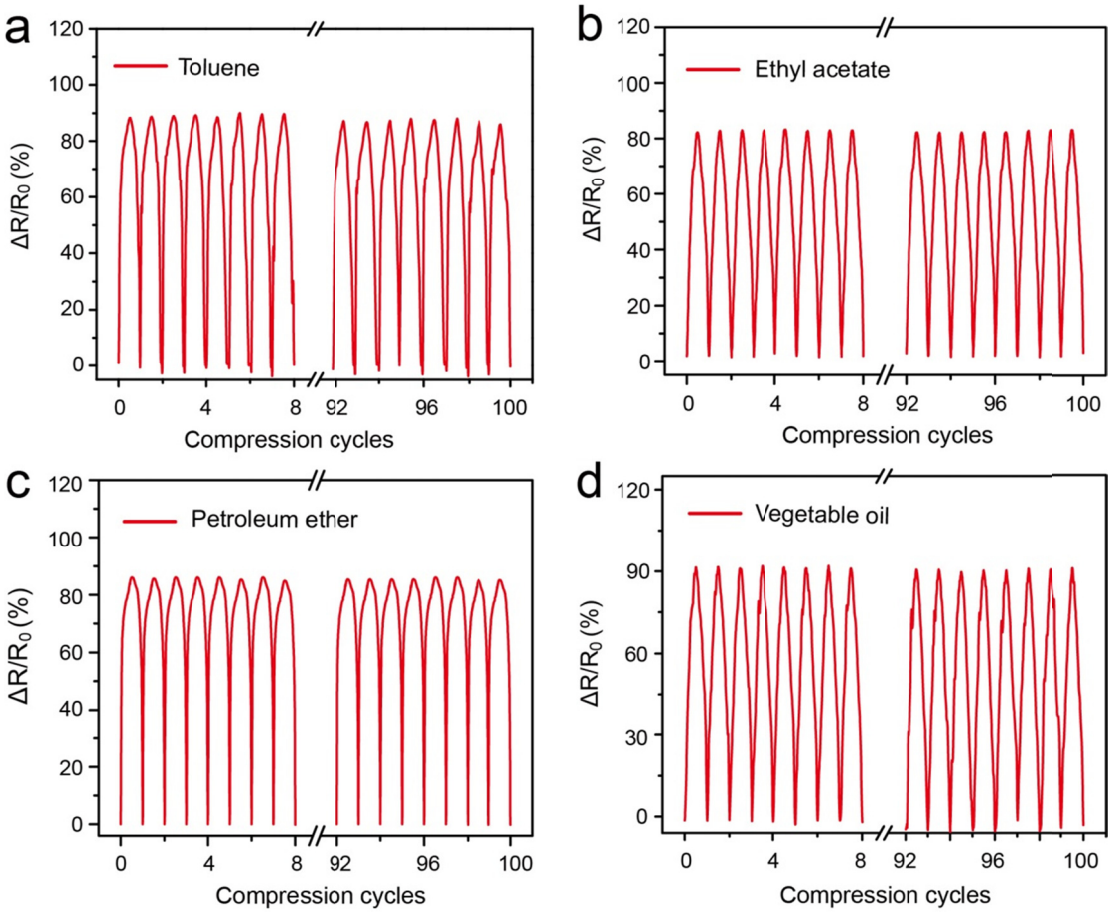

Supplementary Figure 30. $\Delta R/R_0$ during 100 compression cycles at 50% strain in (**a**) toluene, (**b**) ethyl acetate, (**c**) petroleum ether and (**d**) vegetable oil.

Supplementary Table 1. Comparison of the fatigue resistance of the CCAP hydrogel with the previously-reported highly compressible materials.

Materials	**Cycles (strain)**	**Maximum stress retention**	**Residual strain**	**Reference**
CNT film	1000 (57%) 1000 (85%)	77% 63%	7.5% 14%	*Science* 2005, 310, 1307[3]
CNT array	5×10^5 (15%)	53%	5%	*Nat. Nanotech.* 2007, 2, 417[4]
CNT aerogel	100 (60%) 1000 (60%) / Ethanol	100% 114%	17.5% --	*Adv. Mater.* 2010, 22, 617[5]
Hard carbon nanofiber aerogel	10^5 (30%) 10^4 (50%) 10^3 (70%)	98% 93% 74%	1.5% 2% 8%	*Adv. Mater.* 2019, 31, 1900651[6]
Carbon nanofiber aerogel	2×10^6 (20%) 5×10^5 (60%)	99% 96%	0.7% 8%	*Adv. Mater.* 2020, 32, 1904331[7]

Graphene cellular monolith	1000 (50%) 10 (80%)		76% 75%	7% --	*Nat. Commun.* 2012, 3, 1241[8]
Graphene aerogel	1000 (50%)		70%	3%	*Adv. Mater.* 2013, 25, 2219[9]
Graphene aerogel microlattice	10 (50%)		37%	--	*Nat. Commun.* 2015, 6, 6962[10]
Graphene sponge	1000 (90%) 200 (90%) / Acetone		48% 80%	--	*Nat. Commun.* 2015, 6, 6141[11]
Graphene foam	500 (80%)		86%	1%	*Adv. Mater.* 2015, 27, 5943[12]
Lamellar graphene materials	10^6 (20%) 2.5×10^5 (50%)		97% 86%	0.6% 2%	*Nat. Commun.* 2016, 7, 12920[13]
Graphene cellular elastomer	10 (80%)		90%	1%	*Adv. Mater.* 2017, 29, 1701553[14]
Graphene/CNT aerogel	10^6 (2%) 2000 (60%)		100% 100%	0% 0%	*Nat. Nanotech.* 2012, 7, 562[15]
Graphene/CNT aerogel	1000 (50%)		88%	10%	*Adv. Mater.* 2013, 25, 2554[16]
Carbon/rGO aerogel	10^4 (50%)		58%	8.2%	*Adv. Mater.* 2018, 30, 1706705[17]
Graphene-based spring	10^4 (1%)		80%	0%	*Adv. Mater.* 2021, 33, 2102724[18]
Polyacrylonitrile/ SiO_2 aerogel	1000 (60%)		79%	14.5%	*Nat. Commun.* 2014, 5, 5802[19]
Biomass-derived carbon/SiO_2 aerogel	1000 (50%)		75%	4.3%	Adv. Mater. 2016, 28, 9512[20]
Alginate/SiO_2 hydrogel	1000 (50%) / Water		70%	9.5%	*Adv. Mater.* 2017, 29, 1700339[21]
PEDOT/PAMPS/ PAAm hydrogel	4 (90%)		85%	--	*Chem. Mater.* 2014, 26, 3522[22]
CCAP hydrogel	**Air**	**10^5 (15%)**	**93%**	**0.9%**	**This work**
		3×10^4 (50%)	**79%**	**1.5%**	
		500 (70%)	**80%**	**6%**	
	Water	**5×10^5 (15%)**	**97%**	**0%**	
		5×10^4 (50%)	**83%**	**0%**	
		1000 (70%)	**70%**	**3.5%**	
CCAP-based organohydrogel	**Water/ Organic solvents**	**1000 (50%)**	**85%-96%**	**0.4%-4.5%**	
	-50 °C	**100 (50%)**	**80%**	**0%**	

References

1. Li, H.-H. et al. Mixed-PtPd-shell PtPdCu nanoparticle nanotubes templated from copper nanowires as efficient and highly durable electrocatalysts. *Adv. Energy Mater.* **2**, 1182-1187 (2012).

2. Hummers, W. S. & Offeman, R. E. Preparation of graphitic oxide. *J. Am. Chem. Soc.* **80**, 1339-1339 (1958).

3. Cao, A., Dickrell, P. L., Sawyer, W. G., Ghasemi-Nejhad, M. N. & Ajayan, P. M. Super-compressible foamlike carbon nanotube films. *Science* **310**, 1307-1310 (2005).

4. Suhr, J. et al. Fatigue resistance of aligned carbon nanotube arrays under cyclic compression. *Nat. Nanotechnol.* **2**, 417 (2007).

5. Gui, X. et al. Carbon nanotube sponges. *Adv. Mater.* **22**, 617-621 (2010).

6. Yu, Z.-L. et al. Superelastic hard carbon nanofiber aerogels. *Adv. Mater.* **31**, 1900651 (2019).

7. Li, C. et al. Temperature-invariant superelastic and fatigue resistant carbon nanofiber aerogels. *Adv. Mater.* **32**, 1904331 (2020).

8. Qiu, L., Liu, J. Z., Chang, S. L. Y., Wu, Y. Z. & Li, D. Biomimetic superelastic graphene-based cellular monoliths. *Nat. Commun.* **3**, 1241 (2012).

9. Hu, H., Zhao, Z. B., Wan, W. B., Gogotsi, Y. & Qiu, J. S. Ultralight and highly compressible graphene aerogels. *Adv. Mater.* **25**, 2219-2223 (2013).

10. Zhu, C. et al. Highly compressible 3d periodic graphene aerogel microlattices. *Nat. Commun.* **6**, 6962 (2015).

11. Wu, Y. et al. Three-dimensionally bonded spongy graphene material with super

compressive elasticity and near-zero poisson's ratio. *Nat. Commun.* **6**, 6141 (2015).

12. Bi, H., Chen, I.-W., Lin, T. & Huang, F. A new tubular graphene form of a tetrahedrally connected cellular structure. *Adv. Mater.* **27**, 5943-5949 (2015).
13. Gao, H.-L. et al. Super-elastic and fatigue resistant carbon material with lamellar multi-arch microstructure. *Nat. Commun.* **7**, 12920 (2016).
14. Qiu, L. et al. Extremely low density and super-compressible graphene cellular materials. *Adv. Mater.* **29**, 1701553 (2017).
15. Kim, K. H., Oh, Y. & Islam, M. F. Graphene coating makes carbon nanotube aerogels superelastic and resistant to fatigue. *Nat. Nanotechnol.* **7**, 562 (2012).
16. Sun, H. Y., Xu, Z. & Gao, C. Multifunctional, ultra-flyweight, synergistically assembled carbon aerogels. *Adv. Mater.* **25**, 2554-2560 (2013).
17. Zhuo, H. et al. A supercompressible, elastic, and bendable carbon aerogel with ultrasensitive detection limits for compression strain, pressure, and bending angle. *Adv. Mater.* **30**, 1706705 (2018).
18. Gao, H.-L. et al. A highly compressible and stretchable carbon spring for smart vibration and magnetism sensors. *Adv. Mater.* **33**, 2102724 (2021).
19. Si, Y., Yu, J., Tang, X., Ge, J. & Ding, B. Ultralight nanofibre-assembled cellular aerogels with superelasticity and multifunctionality. *Nat. Commun.* **5**, 5802 (2014).
20. Si, Y. et al. Ultralight biomass-derived carbonaceous nanofibrous aerogels with superelasticity and high pressure-sensitivity. *Adv. Mater.* **28**, 9512-9518 (2016).
21. Si, Y. et al. Ultrahigh-water-content, superelastic, and shape-memory nanofiber-assembled hydrogels exhibiting pressure-responsive conductivity. *Adv. Mater.* **29**, 1700339 (2017).

22. Du, G. et al. Tough and fatigue resistant biomimetic hydrogels of interlaced self-assembled conjugated polymer belts with a polyelectrolyte network. *Chem. Mater.* **26**, 3522-3529 (2014).